

# Influence of the free surface reconstruction on the spatial laser energy distribution in high power laser beam welding modeling

Cite as: J. Laser Appl. **34**, 042023 (2022); <https://doi.org/10.2351/7.0000739>

Submitted: 17 June 2022 • Accepted: 08 September 2022 • Published Online: 21 October 2022

 Xiangmeng Meng, Stephen Nugraha Putra,  Marcel Bachmann, et al.

## COLLECTIONS

Paper published as part of the special topic on [Proceedings of the International Congress of Applications of Lasers & Electro-Optics \(ICALEO 2022\)](#)



View Online



Export Citation



CrossMark

## ARTICLES YOU MAY BE INTERESTED IN

[Designing of aluminium case lid of prismatic battery cell for laser powder bed fusion](#)  
Journal of Laser Applications **34**, 042025 (2022); <https://doi.org/10.2351/7.0000743>

[Visualization of cathode spot control using laser irradiation and oxide addition in wire arc additive manufacturing of titanium alloys](#)  
Journal of Laser Applications **34**, 042024 (2022); <https://doi.org/10.2351/7.0000738>


[Evaluation of narrowed weld pool shapes and their effect on resulting potential defects during deep penetration laser beam welding](#)  
Journal of Laser Applications **34**, 042005 (2022); <https://doi.org/10.2351/7.0000733>



**LIA**  
THE LASER INSTITUTE

The professional society for  
lasers, laser applications,  
and laser safety worldwide.

Become part of the LIA experience -  
cultivating innovation, ingenuity, and  
inspiration within the laser community.



MEMBER

[www.lia.org/membership](http://www.lia.org/membership)  
[membership@lia.org](mailto:membership@lia.org)

[Find Out More](#)

# Influence of the free surface reconstruction on the spatial laser energy distribution in high power laser beam welding modeling

Cite as: J. Laser Appl. 34, 042023 (2022); doi: 10.2351/7.0000739

Submitted: 17 June 2022 · Accepted: 8 September 2022 ·

Published Online: 21 October 2022



Xiangmeng Meng,<sup>1</sup> Stephen Nugraha Putra,<sup>1</sup> Marcel Bachmann,<sup>1</sup> Antoni Artinov,<sup>1</sup>   
and Michael Rethmeier<sup>1,2,3</sup>

## AFFILIATIONS

<sup>1</sup>BAM Federal Institute for Materials Research and Testing, Unter den Eichen 87, Berlin 12205, Germany

<sup>2</sup>Institute of Machine Tools and Factory Management, Technical University Berlin, Pascalstraße 8-9, Berlin 10587, Germany

<sup>3</sup>Fraunhofer Institute for Production Systems and Design Technology, Pascalstraße 8-9, 10587 Berlin, Germany

**Note:** Paper published as part of the special topic on Proceedings of the International Congress of Applications of Lasers & Electro-Optics 2022.

## ABSTRACT

An accurate and efficient description of the spatial distribution of laser energy is a crucial factor for the modeling of laser material processing, e.g., laser welding, laser cutting, or laser-based additive manufacturing. In this study, a 3D heat transfer and fluid flow model coupled with the volume-of-fluid algorithm for free surface tracking is developed for the simulation of molten pool dynamics in high-power laser beam welding. The underlying laser-material interactions, i.e., the multiple reflections and Fresnel absorption, are considered by a ray-tracing method. Two strategies of free surface reconstruction used in the ray-tracing method are investigated: a typical piecewise linear interface calculation (PLIC)-based method and a novel localized level-set method. The PLIC-based method is discrete, resulting in non-continuous free surface reconstruction. In the localized level-set method, a continuous free surface is reconstructed, and, thus, the exact reflection points can be determined. The calculated spatial laser energy distribution and the corresponding molten pool dynamics from the two methods are analyzed and compared. The obtained numerical results are evaluated with experimental measurements to assure the validity of the proposed model. It is found that distinct patterns of the beam multiple reflections are obtained with the different free surface reconstructions, which shows significant influence not only on the molten pool behaviors but also on the localized keyhole dynamics.

Key words: laser beam welding, laser energy distribution, weld pool dynamics, ray tracing

© 2022 Author(s). All article content, except where otherwise noted, is licensed under a Creative Commons Attribution (CC BY) license (<http://creativecommons.org/licenses/by/4.0/>). <https://doi.org/10.2351/7.0000739>

## I. INTRODUCTION

The laser beam welding (LBW) performed in the deep-penetration mode, also known as keyhole mode, is considered one of the most important joining processes in industrial applications, especially for the high-efficiency and high-quality joining of thick-walled structures. Due to its extremely concentrated energy input, the LBW shows several attractive advantages compared with typical arc welding processes, such as deeper penetration, higher welding speed, narrower heat affected zone, and finer grain size.<sup>1</sup> The most important characteristic of the deep-penetration LBW is the

formation of a keyhole within the weld pool. Multiple reflections of the laser beam will occur inside the keyhole, and correspondingly the laser energy is absorbed multiple times on the keyhole wall, which in turn further increases the thermal efficiency of the process up to 90%. Therefore, the transient spatial laser energy distribution on the keyhole wall is the underlying factor influencing the keyhole and molten pool dynamics, which further influences the geometry, microstructure, possible defect formation, and, hence, the final properties of the weld seam.

To obtain a better understanding of the physics involved in the LBW process, some experimental attempts have been

performed to visualize the keyhole and molten pool dynamics based on different monitoring and detecting systems, including infrared imaging,<sup>2</sup> high-speed imaging,<sup>3</sup> and synchrotron x-ray measurement.<sup>4</sup> However, quantitative descriptions of the keyhole and molten pool dynamics, especially for the physical information inside the molten pool as well as the laser-keyhole interactions, are still very limited due to difficulties in accessing the internal molten pool, the expensive equipment, and the relatively low image resolution.

With the advancement of computational technologies, sophisticated 3D numerical models coupled with free surface tracking algorithms such as the volume-of-fluid (VOF) method<sup>5</sup> or the level-set (LS) method<sup>6</sup> were developed to investigate the most relevant physical phenomena occurring during the LBW process. Obviously, an accurate and efficient description of the energy coupling between the laser beam and the keyhole is the kernel for the calculation. The commonly used methodologies include predefined keyhole boundary,<sup>7</sup> volumetric heat source,<sup>8,9</sup> ray tracing method,<sup>10,11</sup> and electromagnetic wave equations.<sup>12,13</sup> Among these methods, the ray-tracing method is a physics-based algorithm and provides a good balance between physical accuracy and computational intensity. It focuses on the geometrical relationship between the beam propagation and the keyhole profile by calculating the multiple reflection paths of the laser beam and the laser absorption at each reflection point.

The numerically reconstructed keyhole wall, which is the reflection surface of the laser beam, can, however, not be mathematically described by an explicit or continuous expression. Certain reconstruction (for VOF method) or interpolation methods (for LS method) must be performed to rebuild the free surface, which may cause difficulties when calculating the reflection point and, moreover, to negatively influence the accuracy of the laser energy distribution. For instance, with a VOF-tracked free surface, the piecewise linear interface calculation (PLIC)-based ray-tracing method is the most widely applied algorithm with the least computational intensity. Nonetheless, it is known that two major issues will be produced from the geometrical aspects, i.e., the unphysical capture of the rays and the numerical leakage of the rays, leading to unacceptable calculation errors, especially for a higher welding speed above 3 m/min.<sup>14,15</sup>

Although it has been preliminarily recognized that the calculated spatial laser energy distribution is highly dependent on the correlation between the free surface reconstruction and the ray-tracing algorithm, the influences of different reconstruction methods on the laser-keyhole interaction and resultant keyhole and molten pool dynamics have not been studied systematically. In this paper, two types of free surface reconstruction methods are chosen to cooperate with the ray-tracing algorithm: a typical PLIC-based method and a novel localized LS method. The laser beam propagation and the laser absorption with different algorithms are visualized and analyzed. The resultant keyhole dynamics and molten pool behavior are compared in detail.

## II. MATHEMATICAL MODELING

### A. Ray-tracing algorithms

To calculate the multiple reflections of the laser beam on the complex-shaped and time-varying keyhole surface, the laser beam

is discretized into a sufficient number of sub-rays (697 sub-rays in this study). The energy density of each sub-ray is determined by its relative location to the optical axis, which is expressed as

$$q_L(x, y) = \frac{2P_L}{\pi r_f^2} \exp\left(-2 \frac{x^2 + y^2}{r_f^2}\right), \quad (1)$$

where  $P_L$  is the laser power and  $r_f$  is the laser beam radius.

The initial sub-ray path  $\vec{I}_0$  is defined by considering the divergence feature of the laser beam, which is given as

$$r_f(z) = r_{f0} \left[ 1 + \left( \frac{z - z_0}{z_r} \right)^2 \right]^{1/2}, \quad (2)$$

where  $r_{f0}$  is the beam radius at the focal plane,  $z_0$  is the position of the focal plane, and  $z_r$  is the Rayleigh length.

The direction of the reflected sub-ray that is also the incident ray for the next reflection can be determined by the following geometrical relationship:

$$\vec{R}_0 = \vec{I}_1 = \vec{I}_0 - 2(\vec{I}_0 \cdot \vec{N}_0)\vec{N}_0, \quad (3)$$

where  $\vec{R}_0$  is the reflected direction and  $\vec{N}_0$  is the outward normal vector at the reflection points on the keyhole wall.

The Hagen–Rubin’s model is employed to calculate the absorption rate at the reflection points, which is a function of the incident angle,  $\theta_n$ , and the material-dependent coefficient  $\varepsilon$ ,

$$\alpha = 1 - \frac{1}{2} \left( \frac{1 + (1 - \varepsilon \cos \theta_n)^2}{1 + (1 + \varepsilon \cos \theta_n)^2} + \frac{\varepsilon^2 - 2\varepsilon \cos \theta_n + 2\cos^2 \theta_n}{\varepsilon^2 + 2\varepsilon \cos \theta_n + 2\cos^2 \theta_n} \right). \quad (4)$$

A schematic of the beam discretization and the multiple reflections is given in Fig. 1. Apparently, finding the accurate locations of the reflection points on the keyhole wall, namely, the intersection between the propagating sub-rays and the complicated keyhole geometry, is critical to the ray-tracing algorithm.

### 1. PLIC-based ray-tracing algorithm

The VOF-tracked keyhole profile is not originally explicit; in other words, the volume fraction  $F$  and its gradient  $\nabla F$ , i.e., the normal vector of the free surface, are not sufficient for a direct determination of the reflection points. Instead, a discriminant criterion is commonly applied, as shown in Fig. 2(a).  $d_{ray}$  is the distance between the center of the free surface cell and the incident ray  $\vec{I}_0$  and  $r_{sp}$  is the radius of the circumscribed sphere of the cell. A free surface cell will be selected as the reflection cell if the following discriminant is fulfilled, and the cell center will be considered the reflection point,<sup>16</sup>

$$d_{ray} \leq r_{sp}, \quad (5)$$

$$d_{ray} = |\vec{P}_0 \vec{P}_1| \sin \left( \arccos \left( \frac{|\vec{P}_0 \vec{P}_1 \cdot \vec{I}_0|}{|\vec{P}_0 \vec{P}_1| |\vec{I}_0|} \right) \right). \quad (6)$$

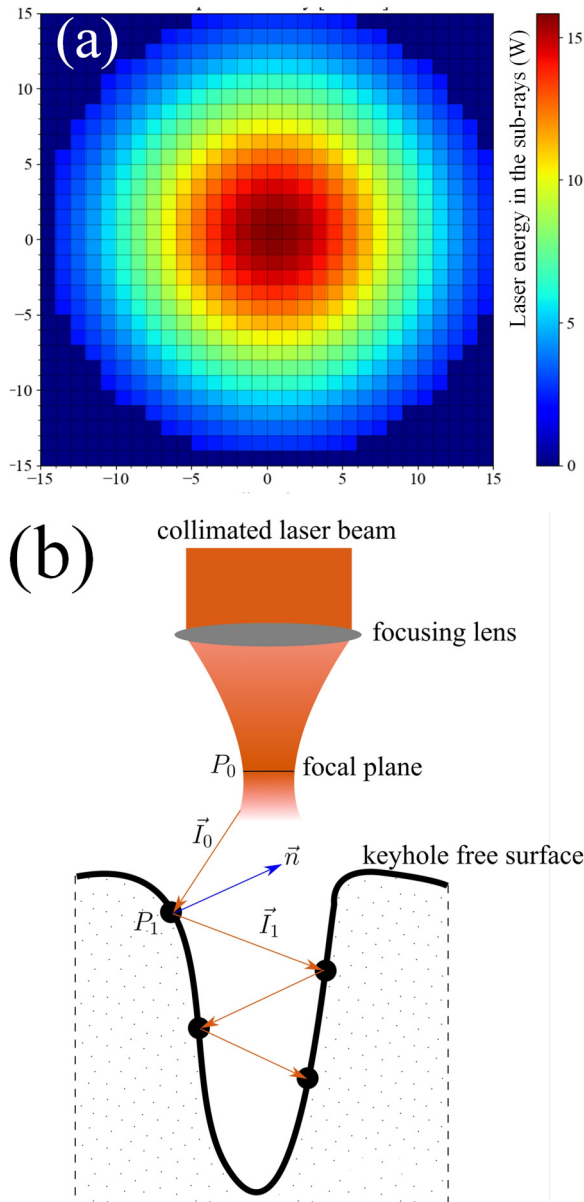


FIG. 1. Schema of the basic principle of the ray-tracing approach: (a) beam discretization, (b) multiple reflections.

From Eqs. (5) and (6), it can be seen that the accuracy of the ray-tracing algorithm is dependent on the cell size used to discretize the computational domain. Considering the laser spot size of several hundred micrometers, a mesh size below  $100\ \mu\text{m}$  should be chosen for a trustable calculation of the multiple reflections. However, this extremely fine mesh size will lead to unaffordable calculation intensity for the subsequent computational fluid dynamics (CFD) simulation.

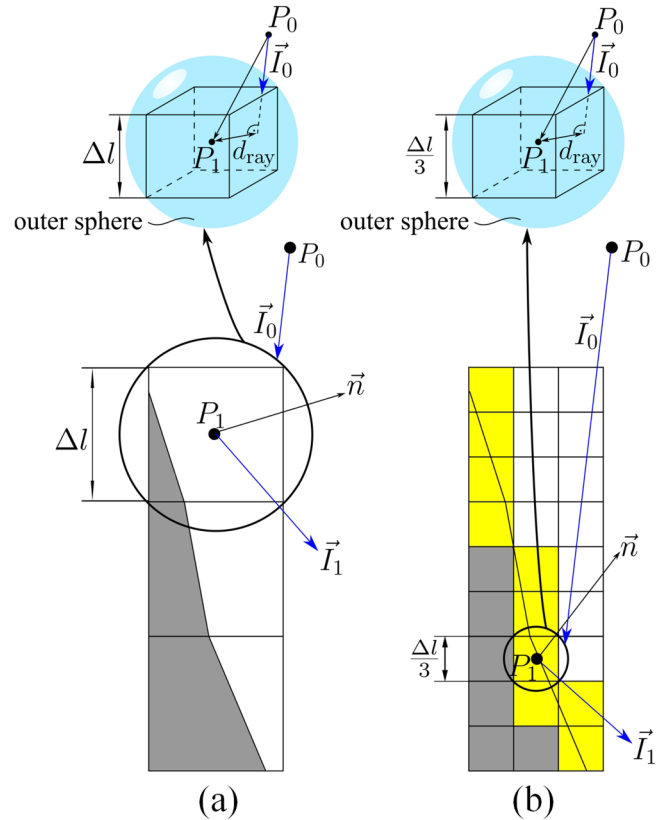


FIG. 2. Schematic of the PLIC-based ray-tracing methods: (a) without virtual refinement, (b) with refinement.

## 2. PLIC-based ray-tracing algorithm with virtual refinement

A virtual refinement strategy was proposed by Cho *et al.* and integrated with the original ray-tracing algorithm described above, as shown in Fig. 2(b). By using the volume fraction  $F$  and its gradient  $\nabla F$ , the distance from the cell center to the free surface constructed by the PLIC algorithm can be determined.<sup>10</sup> By taking the cell center as the origin, the mathematical equation of the free surface can be written as

$$n_x x + n_y y + n_z z = d_{\text{center}}, \quad (7)$$

where  $d_{\text{center}}$  is the distance from the free surface to the cell center and  $n_x$ ,  $n_y$ , and  $n_z$  are the  $x$ ,  $y$ , and  $z$  components of  $\nabla F$ .

Subsequently, the free surface is divided into virtual cells of sufficiently small size (less than  $50\ \mu\text{m}$  in this study). The virtual cells that are located on the free surface can be identified using Eq. (7). Therefore, a smaller  $r_{\text{sp}}$  can be used to determine the virtual reflection cell, which results in higher accuracy of the calculated reflection position. These virtual cells are only used for the

calculation of the beam propagation and are not involved in the CFD simulation, bringing almost no additional computational load.

### 3. Ray-tracing algorithm with localized LS method

The VOF and LS advection equations can be fully coupled, namely, the Coupled LSVOF method, to calculate a continuous and smooth free surface; meanwhile, the conservation of mass can also be guaranteed. However, the coupled LSVOF method usually requires extremely small time steps, which may lead to an unacceptable calculation time for a transient model. In this study, a localized LS method proposed by Sun and Tao<sup>17</sup> is applied to reconstruct the VOF-tracked free surface. The LS functions are derived from the geometric operation of the volume fraction data, without solving the real LS advection equation.

The signed distance from the cell node to the free surface, expressed by Eq. (7), can be calculated as follows:

$$d_{\text{node}} = \begin{cases} -(n_x x + n_y y + n_z z) - d_{\text{center}} & F \leq 0.5, \\ -(n_x x + n_y y + n_z z) + d_{\text{center}} & F \geq 0.5. \end{cases} \quad (8)$$

A positive distance represents that the node is in the gas phase and a negative value represents a position within the molten metal. A node may have multiple signed distances according to the different free surface equations from the surrounding cells, as shown in Fig. 3(a). The unique signed distance  $\Phi$ , i.e., the LS function value, is selected as the largest absolute value from the candidates. After determining all the  $\Phi$  values at the nodes of a cell, the free surface inside the cell can be reconstructed as the iso-surface  $\Phi(x, y, z) = 0$  by a trilinear interpolation, as given in Fig. 3(b).

By writing the incident ray as a parametric equation of  $t$ ,  $P_1 = P_0 + t\vec{I}_0$ , and combing with the reconstructed LS iso-surface  $\Phi(x, y, z) = 0$ , the intersection between the sub-ray and the free surface, i.e., the exact reflection point, can be obtained, see Fig. 4.<sup>14</sup>

## B. Numerical modeling of LBW

In this study, a 3D transient heat transfer and fluid flow model coupled with free surface tracing is developed for the calculation of keyhole dynamics and molten pool behavior in LBW of stainless steel. The flow regime in the molten pool is considered laminar, and the fluid is assumed as Newtonian and incompressible.

The transient geometries of the keyhole and the molten pool free surface are tracked with the VOF method, requiring dual phases (Ar and metal) in the model. The laser energy input calculated by the ray-tracing algorithm together with the energy dissipation due to convection, radiation, and evaporation is employed in the model for the calculation of the temperature field. The recoil pressure as a function of the local temperature<sup>18</sup> is applied to the keyhole wall. The dynamic balance between recoil pressure, hydrostatic pressure, hydrodynamic pressure, and Laplace pressure should be calculated to determine the transient keyhole geometry. The solid and liquid metal is treated as a single phase, and the solid/liquid phase transformation is considered by the enthalpy-porosity method to calculate the boundary of the molten pool. An additional braking force based on the Carman-Kozeny equation is added to the semi-solid region for the flow deceleration.<sup>19</sup> The

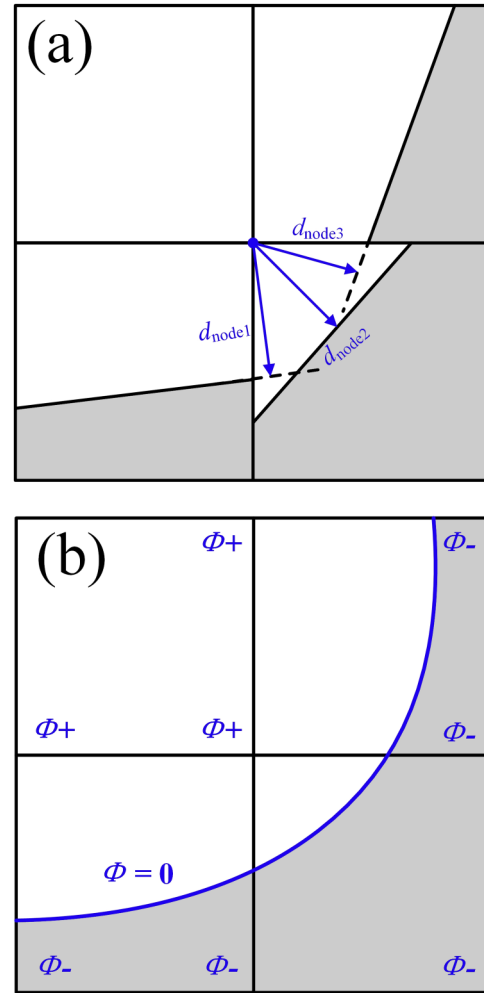


FIG. 3. Schematic of the localized LS algorithm: (a) definition of the signed distance  $\Phi$ .

thermo-capillary flow driven by the steep temperature gradient on the top surface of the molten pool and the buoyancy based on the Boussinesq approximation are considered as well.

The detailed descriptions of the physical models, boundary conditions, numerical considerations, etc. can be found in the authors' previous studies.<sup>20,21</sup>

## III. EXPERIMENTAL SETUPS

Bead-on-plate welding experiments were conducted to obtain validation data for the model. An austenitic AISI 304 stainless steel was utilized as the base metal, and the dimensions of the workpiece were  $200 \times 60 \times 10 \text{ mm}^3$ . A Trumpf disk laser system with a maximum output of 16 kW was used as the laser source. The corresponding optical parameters of the laser are listed in Table I.

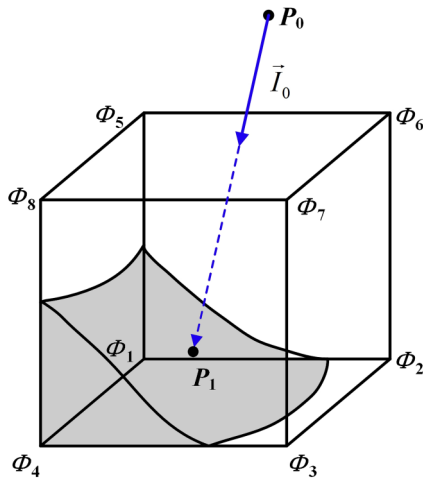


FIG. 4. Schema of the calculation of the intersection between reconstructed LS surface and sub-ray.

The welding experiments were performed with a laser power of 4.0 kW and a welding speed of 1.0 m/min. Pure argon with 20 l/min flow rate was provided behind the laser spot to protect the weld seam from oxidation. Mechanical cleaning on the workpiece surface was performed before welding.

The obtained weld specimens were mechanically cut, ground, and polished on the cross section, and subsequently etched with a V2A etchant (100 ml H<sub>2</sub>O, 100 ml HNO<sub>3</sub>, and 10 ml HCl). An optical microscope was used to observe the fusion line shape on the cross section.

#### IV. RESULTS AND DISCUSSION

First, a benchmark is performed to evaluate the performance of the different ray-tracing algorithms with the same predefined keyhole profiles, as shown in Fig. 5. The multiple reflection paths of the sub-rays are visualized for a better intuition. For the PLIC-based ray-tracing method, the reflections can only be built between the cell center, see Fig. 2(a). Therefore, all sub-rays reflect between a few cells at the keyhole bottom, obviously not following the optical rules. With the introduced virtual refinement strategy, the issue of the physically unreasonable reflections is mitigated, and the sub-rays reflect more irregularly at the bottom of the keyhole, more precisely, between the center of the virtual cells, as shown in Fig. 5(b). In

TABLE I. Laser parameters used in experiment and simulation.

Laser parameters	Value
Laser spot radius at focal plane	0.21 mm
Wavelength	1040 nm
Focal position	-3.0 mm
Rayleigh length	3.6 mm

contrast, the exact reflection points can be located on the LS-reconstructed free surface. The combination of the divergence feature of the laser beam and the complicated keyhole geometry leads to an extremely irregular reflection pattern inside the keyhole, which produces a different energy distribution on the keyhole wall.

The simulated molten pool shape and the velocity field for the real welding experiment (laser power 4 kW, welding speed 1 m/min) are provided in Fig. 6, together with the time-averaged spatial distribution of the absorbed laser heat flux (within 0.2 s). As seen, the energy distribution from the different ray-tracing methods with different reflection strategies shows a significant influence on the keyhole and molten pool dynamics. A strong counterclockwise circulation forms in the bottom region of the molten pool,

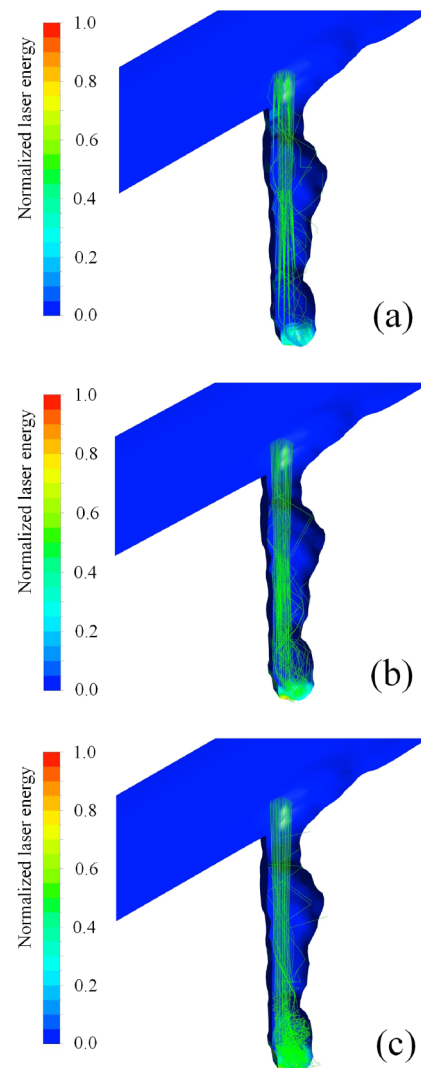
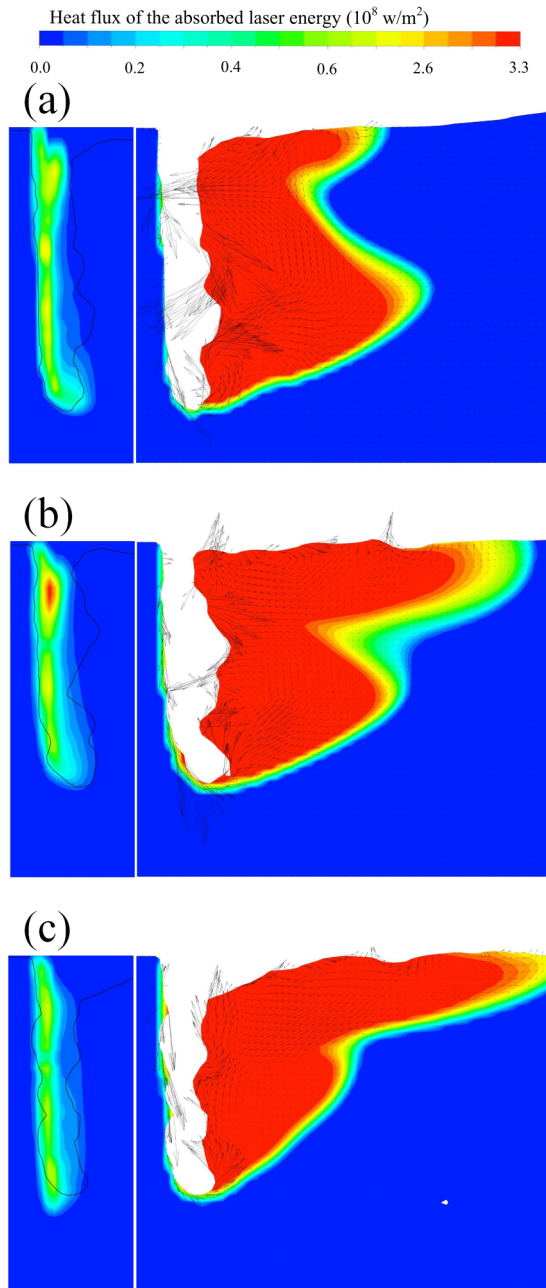
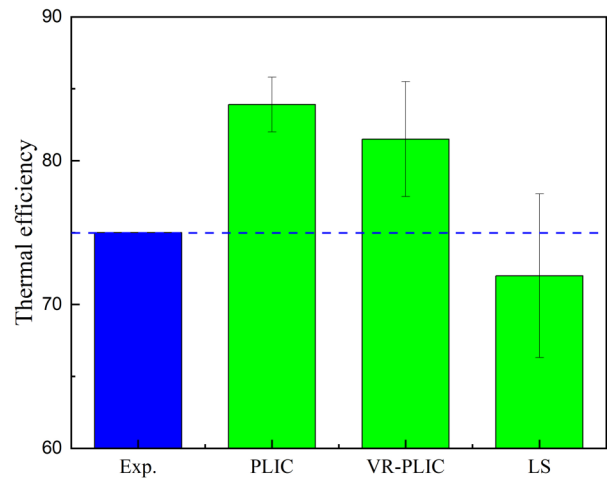


FIG. 5. Visualization of the multiple reflections of the sub-rays: (a) PLIC-based, (b) PLIC-based with virtual refinement, (c) LS-based.



**FIG. 6.** Calculated (left side) time-averaged absorbed laser energy and (right side) the molten pool dynamics: (a) PLIC-based, (b) PLIC-based with virtual refinement, (c) LS-based.

enlarging the liquid metal volume at the weld pool bottom, as shown in Fig. 6(a). The top region of the molten pool is, however, unreasonably small. This calculated molten pool shape is currently not supported by the experimental observations<sup>4</sup> or the calculations



**FIG. 7.** Calculated thermal efficiency from different ray-tracing algorithms.

from other researchers.<sup>10</sup> The calculated molten pool from the virtual refinement enhanced ray-tracing method and the LS-based ray-tracing method shows the common geometry, i.e., elongated at the top region and relatively shorter at the bottom region, which is well experimentally and numerically confirmed.<sup>4,10</sup>

Distinct characteristics of the keyhole front wall behavior are also identified, especially for the formation and movement of the small swellings thereon. The small swellings are considered to have a significant influence on the laser energy absorption as well as the beam propagation inside the keyhole.<sup>22</sup> The size of the swellings is the magnitude of hundreds of micrometers, which is close to the commonly used mesh size for CFD calculation of the LBW process; thus, this delicate behavior cannot be revealed reasonably by the typical PLIC-based ray-tracing method whose criterion is based on the mesh size. More swellings are formed on the keyhole front wall with the LS-based ray-tracing algorithm, and correspondingly more energy is absorbed by the front keyhole wall since the exact reflection position of the sub-rays on the swelling can be located.

According to the experimental measurements from Kawahito *et al.*, the thermal efficiency of the laser beam welding process in keyhole mode shows an approximately linear relationship with the penetration depth,<sup>23</sup> and the thermal efficiency can reach 75% with a penetration depth of about 8 mm. The thermal efficiency of the calculated welding process is plotted in Fig. 7, and the standard deviation represents the fluctuation of the heat input induced by dynamic keyhole evolution. The PLIC-based ray-tracing method provides the highest thermal efficiency of 83.9% with the highest relative error of 12%. The overestimation is caused by the unphysical capture and absorption of the rays from the inaccurate capturing criterion. The application of virtual refinement improves the accuracy of the calculation for laser absorption. The obtained result from the LS-based ray-tracing method shows the best agreement with the experimental value with a relative error of 4.9%. It is worth noting that the LS-based ray-tracing method also provides the highest standard deviation of the thermal efficiency among the

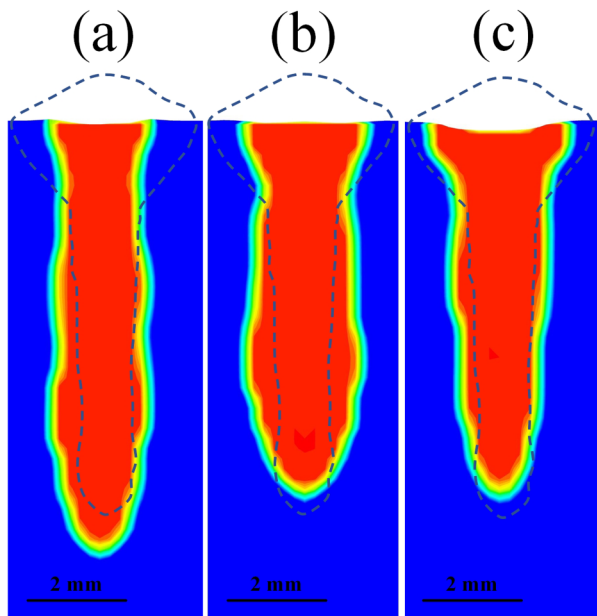


**FIG. 8.** Comparison of fusion line shapes between numerical and experimental results: (a) PLIC-based, (b) PLIC-based with virtual refinement, (c) LS-based.

three cases. It is deduced that the simulated keyhole experiences the severest fluctuation.

To evaluate the validity of the three models, the simulated fusion lines are compared with the experimental results, as given in Fig. 8. Due to the overestimated heat input from the PLIC-based ray-tracing method, the calculated penetration depth is also larger than the experimental value. It also confronts one common difficulty in the simulation of the partial penetration LBW, i.e., the reproduction of the so-called wine-glass shape at the top region.<sup>24,25</sup> Some additional heat sources have to be introduced when trying to reproduce this particular profile.<sup>10,26</sup> With the virtual refinement strategy, an accurate penetration depth can be obtained, but the calculated weld has a swelling in the bottom region; in contrast, the experimental weld is narrow and parallel. The results from the LS-based ray-tracing method show the most accurate prediction, in which not only the deep and parallel weld geometry but also the wine-glass profile is reproduced successfully.

## V. CONCLUSIONS

In this study, three ray-tracing algorithms based on different free surface reconstruction strategies are developed and integrated into a CFD model of the laser beam welding process. The calculated beam propagation inside the keyhole, the spatial distribution of the laser energy, and the resultant molten pool dynamics are evaluated and compared. The main conclusions are drawn below:

1. Due to the different determination strategies of the reflection points in PLIC-based and LS-based methods, distinct patterns

of the beam multiple reflections are obtained, leading to the different spatial distribution of the laser energy.

2. The selection of the ray-tracing algorithm shows significant influence not only on the general molten pool behaviors but also on the localized keyhole dynamics, e.g., the formation and movement of the swellings on the keyhole front wall.
3. By comparing the experimental results and the data from the literature, it is found that the PLIC-based ray-tracing method has the least accuracy in predicting the thermal efficiency and the final fusion line of the weld. The application of the virtual refinement technique can improve the calculation results to some extent, but the derivation is still noticeable. The LS-based ray-tracing method provides the best agreement with the available experimental data.

## ACKNOWLEDGMENT

This work is funded by the Deutsche Forschungsgemeinschaft (DFG, German Research Foundation)—Project No. 416014189.

## AUTHOR DECLARATIONS

### Conflict of Interest

The authors have no conflicts to disclose.

## Author Contributions

**Xiangmeng Meng:** Conceptualization (equal); Data curation (equal); Formal analysis (equal); Investigation (equal); Methodology (equal); Software (equal); Supervision (equal); Validation (equal); Visualization (equal); Writing – original draft (lead); Writing – review & editing (equal). **Stephen Nugraha Putra:** Data curation (lead); Formal analysis (equal); Investigation (equal); Methodology (equal); Writing – review & editing (supporting). **Marcel Bachmann:** Conceptualization (equal); Formal analysis (supporting); Funding acquisition (lead); Project administration (lead); Supervision (equal); Writing – review & editing (equal). **Antoni Artinov:** Formal analysis (supporting); Writing – review & editing (equal). **Michael Rethmeier:** Supervision (lead); Writing – review & editing (equal).

## REFERENCES

- <sup>1</sup>M. Rethmeier, A. Gumenyuk, and M. Bachmann, “High-power laser beam welding for thick section steels—New perspectives using electromagnetic systems,” *Sci. Technol. Weld. Joining* **27**, 43–51 (2022).
- <sup>2</sup>J. Wang, H. Yu, Y. Qian, and R. Yang, “Interference analysis of infrared temperature measurement in hybrid welding,” in *Robotic Welding, Intelligence and Automation* (Springer, Berlin, 2011), pp. 369–374.
- <sup>3</sup>A. Artinov, N. Bakir, M. Bachmann, A. Gumenyuk, S.-J. Na, and M. Rethmeier, “On the search for the origin of the bulge effect in high power laser beam welding,” *J. Laser Appl.* **31**, 022413 (2019).
- <sup>4</sup>Y. Kawahito *et al.*, “Elucidation of the effect of welding speed on melt flows in high-brightness and high-power laser welding of stainless steel on basis of three-dimensional X-ray transmission *in situ* observation,” *Weld. Int.* **31**, 206–213 (2017).
- <sup>5</sup>A. Otto, H. Koch, K.-H. Leitz, and M. Schmidt, “Numerical simulations—A versatile approach for better understanding dynamics in laser material processing,” *Phys. Procedia* **12**, 11–20 (2011).



- <sup>6</sup>J. Chen, X. Chen, X. Liu, and Y. Wei, "Numerical investigation on keyhole collapsing and rebuilding behavior during pulsed laser beam welding of Ti6Al4V titanium alloy under various pulse frequencies," *Appl. Phys. A* **128**, 140 (2022).
- <sup>7</sup>A. Kaplan, "A model of deep penetration laser welding based on calculation of the keyhole profile," *J. Phys. D: Appl. Phys.* **27**, 1805–1814 (1994).
- <sup>8</sup>T. F. Flint, J. A. Francis, M. C. Smith, and J. Balakrishnan, "Extension of the double-ellipsoidal heat source model to narrow-groove and keyhole weld configurations," *J. Mater. Process. Technol.* **246**, 123–135 (2017).
- <sup>9</sup>F. Lu, X. Li, Z. Li, X. Tang, and H. Cui, "Formation and influence mechanism of keyhole-induced porosity in deep-penetration laser welding based on 3D transient modeling," *Int. J. Heat Mass Transfer* **90**, 1143–1152 (2015).
- <sup>10</sup>W.-I. Cho, S.-J. Na, C. Thomy, and F. Vollertsen, "Numerical simulation of molten pool dynamics in high power disk laser welding," *J. Mater. Process. Technol.* **212**, 262–275 (2012).
- <sup>11</sup>S. Pang, L. Chen, J. Zhou, Y. Yin, and T. Chen, "A three-dimensional sharp interface model for self-consistent keyhole and weld pool dynamics in deep penetration laser welding," *J. Phys. D: Appl. Phys.* **44**, 025301 (2011).
- <sup>12</sup>M. Courtois, M. Carin, P. Le Masson, S. Gaied, and M. Balabane, "A complete model of keyhole and melt pool dynamics to analyze instabilities and collapse during laser welding," *J. Laser Appl.* **26**(4), 042001 (2014).
- <sup>13</sup>M. Courtois, M. Carin, P. Le Masson, S. Gaied, and M. Balabane, "A new approach to compute multi-reflections of laser beam in a keyhole for heat transfer and fluid flow modelling in laser welding," *J. Phys. D: Appl. Phys.* **46**, 505305 (2013).
- <sup>14</sup>J. Ahn and S.-J. Na, "Three-dimensional thermal simulation of nanosecond laser ablation for semitransparent material," *Appl. Surf. Sci.* **283**, 115–127 (2013).
- <sup>15</sup>A. Artinov, X. Meng, M. Bachmann, and M. Rethmeier, "Numerical analysis of the partial penetration high power laser beam welding of thick sheets at high process speeds," *Metals* **11**, 1319 (2021).
- <sup>16</sup>J.-H. Cho and S.-J. Na, "Implementation of real-time multiple reflection and Fresnel absorption of laser beam in keyhole," *J. Phys. D: Appl. Phys.* **39**, 5372–5378 (2006).
- <sup>17</sup>D. L. Sun and W. Q. Tao, "A coupled volume-of-fluid and level set (VOSET) method for computing incompressible two-phase flows," *Int. J. Heat Mass Transfer* **53**, 645–655 (2010).
- <sup>18</sup>V. Semak and A. Matsunawa, "The role of recoil pressure in energy balance during laser materials processing," *J. Phys. D: Appl. Phys.* **30**, 2541–2552 (1997).
- <sup>19</sup>V. R. Voller and C. Prakash, "A fixed grid numerical modelling methodology for convection-diffusion mushy region phase-change problems," *Int. J. Heat Mass Transfer* **30**, 1709–1719 (1987).
- <sup>20</sup>X. Meng, M. Bachmann, A. Artinov, and M. Rethmeier, "The influence of magnetic field orientation on metal mixing in electromagnetic stirring enhanced wire feed laser beam welding," *J. Mater. Process. Technol.* **294**, 117135 (2021).
- <sup>21</sup>X. Meng, A. Artinov, M. Bachmann, Ö. Üstündağ, A. Gumenyuk, and M. Rethmeier, "The detrimental molten pool narrowing phenomenon in wire feed laser beam welding and its suppression by magnetohydrodynamic technique," *Int. J. Heat Mass Transfer* **193**, 122913 (2022).
- <sup>22</sup>J. Pocorni, S.-W. Han, J. Cheon, S.-J. Na, A. F. H. Kaplan, and H.-S. Bang, "Numerical simulation of laser ablation driven melt waves," *J. Manuf. Process.* **30**, 303–312 (2017).
- <sup>23</sup>Y. Kawahito, N. Matsumoto, Y. Abe, and S. Katayama, "Relationship of laser absorption to keyhole behavior in high power fiber laser welding of stainless steel and aluminum alloy," *J. Mater. Process. Technol.* **211**, 1563–1568 (2011).
- <sup>24</sup>S. Muhammad, S.-W. Han, S.-J. Na, A. Gumenyuk, and M. Rethmeier, "Study on the role of recondensation flux in high power laser welding by computational fluid dynamics simulations," *J. Laser Appl.* **30**, 012013 (2018).
- <sup>25</sup>S. Pang, X. Chen, X. Shao, S. Gong, and J. Xiao, "Dynamics of vapor plume in transient keyhole during laser welding of stainless steel: Local evaporation, plume swing and gas entrapment into porosity," *Opt. Lasers Eng.* **82**, 28–40 (2016).
- <sup>26</sup>Y. Ai, P. Jiang, X. Shao, P. Li, and C. Wang, "A three-dimensional numerical simulation model for weld characteristics analysis in fiber laser keyhole welding," *Int. J. Heat Mass Transfer* **108**, 614–626 (2017).